Next-generation diamond cell and applications to single-crystal neutron diffraction

Bianca Haberl[1,*], Sachith Dissanayake[1], Yan Wu[1], Dean A.A. Myles[1], Antonio M. dos Santos[1], Mark Loguillo[1], Gerald M. Rucker[1], Douglas P. Armitage[1], Malcolm Cochran[1], Katie M. Andrews[1], C. Hoffmann[1], Huibo Cao[1], Masaaki Matsuda[1], Flora Meilleur[1,2], Feng Ye[1], Jamie J. Molaison[1], Reinhard Boehler[1,3]

[1]*Neutron Scattering Division, Neutron Sciences Directorate, Oak Ridge National Laboratory, Oak Ridge, TN 37831, USA*

[2]*Department of Molecular and Structural Biochemistry, North Carolina State University, Raleigh, NC 27695, USA*

[3]*Geophysical Laboratory, Carnegie Institution for Sciences, Washington DC 20015, USA*

*Corresponding author: haberlb@ornl.gov

Abstract

A diamond cell optimized for single-crystal neutron diffraction is described. It is adapted for work at several of the single-crystal diffractometers of the Spallation Neutron Source and the High Flux Isotope Reactor at the Oak Ridge National Laboratory. A simple spring design improves portability across the facilities and affords load maintenance from offline pressurization and during temperature cycling. Compared to earlier prototypes, pressure stability of polycrystalline diamond (Versimax®) has been increased through double-conical designs and ease of use has been improved through changes to seat and piston set-ups. These anvils allow ~30-40% taller samples than possible with comparable single-crystal anvils. Hydrostaticity and the important absence of shear pressure gradients has been established with the use of glycerin as pressure medium. Large single-crystal synthetic diamonds have also been used for the first time with such a clamp-DAC for pressures close to 20 GPa. The cell is made from a copper beryllium alloy and sized to fit into ORNL's magnets for future ultra-low temperature and high-field studies. We show examples from the Spallation Neutron Source's SNAP and CORELLI beamlines and the High Flux Isotope Reactor's HB-3A and IMAGINE beamlines.

1. Introduction

In situ single-crystal neutron scattering under pressure is a key technique for the study of quantum materials as well as other material and planetary sciences. Specifically for quantum materials, it can quantify the changes occurring in their magnetic phase diagram. In contrast to powder diffraction, single-crystal diffraction is more apt to detect faint magnetic signals, monitor weak distortions or deal with complex crystal structures. Significant efforts are therefore underway at Oak Ridge National Laboratory's Spallation Neutron Source (SNS) and High Flux Isotope Reactor (HFIR) to develop and optimize high pressure capabilities for single crystals to allow for 10 GPa under hydrostatic compression.

The diamond anvil cell (DAC) is the device of choice for *in situ* high pressure single-crystal diffraction at the synchrotron, [1,2 and refs therein] and highly sophisticated cells with large diffraction apertures have been developed [3,4]. In contrast, a wide variety of pressure cells is used at neutron sources to accommodate the large sample sizes typically needed. Some classic examples of device types at neutron facilities around the world include gas pressure cells (P_{max}~0.7 GPa), clamp cells (P_{max}~2 GPa), and the Paris-Edinburgh presses (P_{max}~20 GPa) (see for example [5] and refs therein). Another cell used to ~7 GPa at ORNL has been the cubic palm cell [6]. Common to these cells is that either their pressure is limited or they are too large to easily cool to ultra-low temperatures and/or be fitted into magnets for simultaneous high field studies. The diamond cell and other gem cells aim to overcome both these shortcomings.

Single-crystal studies with neutron diamond cells and other gem cells commenced in the 1980s. A sapphire anvil cell was built for X-ray and neutron four-circle diffractometers and employed to ~2.5 GPa for neutron diffraction [7,8]. Nowadays, a "hybrid" sapphire/tungsten carbide gem cell is in use to ~3.5 GPa [9]. Furthermore, a feasibility test at ambient pressure using a panoramic cell with very large moissanite anvils demonstrated successful Laue diffraction on VIVALDI [10]. To achieve significantly higher pressures, diamonds are required over other gems, however.

Neutron diamond anvil cells were developed at the Kurchatov Institute in Moscow by V.A. Somenkov *et al.* and later transferred and further improved by Goncharenko *et al.* in France. The experiments were typically conducted with a liquid (methanol:ethanol mixture) pressure medium to improve hydrostaticity and avoid sample breakage [Ref. 5,11 and Refs. therein]. Indeed, such DAC work was also instrumental in the determination of the lattice parameters and equation of state of hydrogen (deuterium) to ~30 and ~40 GPa, respectively [12,13]. Very recently, several studies on single crystals in diamond anvil cells have been performed across several neutron facilities. A feasibility study at ANSTO's KOALA, a neutron Laue diffractometer, used a Merrill-Basset-type diamond cell with conical Boehler anvils (ø 1 mm culet). It demonstrated sufficient data quality for refinement on crystals of typical X-ray diffraction sizes [14]. Furthermore, at MLZ's four-circle diffractometer HEiDi, monochromatic neutron diffraction was performed in a panoramic DAC with conical Boehler anvils and achieved high-quality data under compression to 1 GPa. Another successful test of cell/anvil set-up with 1.5 mm culets reached 7 GPa [15]. Larger samples (and thus larger culet sizes) require extraordinary loads

upwards of 10 tons applied on the anvil and clamped in with the cell body. This can typically only be achieved through anvils with elaborate support or through the use of ultra-large synthetic diamonds and custom-made, precision-machined cells and gaskets [16-18].

Here, we describe a wide-angle neutron diamond cell that is adapted for single-crystal diffraction across several beamlines at SNS and HFIR. Similar to the previously at ORNL developed wide-angle and SNAP DACs, [17,18], the cell boasts a wide-angle aperture, a spring mechanism for locking-in of pressure and anvils in the more stable conical design. Using single-crystal diamonds grown by chemical vapor deposition (CVD), a maximum pressure of close to 20 GPa has successfully been locked-in. Furthermore, testing of cell and pressure media with polycrystalline diamond (Versimax®) suggests strongly that the current set-up is capable of hydrostatic pressures on ~0.7 x 0.7 x 0.2 mm^3 single crystals up to ~10 GPa. This large sample size is enabled by the Versimax® anvils that allow for larger gasket thickness than single-crystal anvils. Absence of shear gradients to ~10 GPa is ensured through the use of deuterated glycerin as pressure transmitting medium, a higher useful pressure regime than reported in the past. Moreover, the DAC including the spring is entirely made from non-magnetic copper beryllium and is designed with an outer diameter that could fit into existing ORNL magnets. In future, this design may permit the measurement of samples under pressure and simultaneous high field at ultra-low temperatures. Finally, the cell is straightforward to maintain and prepare and is highly portable. It will thus be incorporated in the Sample Environment Group and be available in the general user program.

2. High pressure at ORNL's single-crystal diffractometers

The diamond cell is adaptable for four different single-crystal diffractometers at SNS and HFIR. A full review of the single-crystal diffraction (SCD) instrument suite is given elsewhere in this issue; here we solely highlight relevant details for pressure application.

Two main groups of instruments can be distinguished by using a monochromatic beam (e.g. HB-3A) versus a polychromatic neutron beam. The instruments with polychromatic beam, comprised of a band of neutron wavelengths, are subdivided into two groups, namely Laue (e.g. IMAGINE) and wavelength-resolved Laue diffractometers (e.g. SNAP and CORELLI).

The HB-3A beamline at HFIR, represents the sole monochromatic diffractometer for high pressure studies under DACs. Its flexible monochromator setting allows three incident neutron wavelengths for various reciprocal space Q coverages and tailors the instrument's sensitivity to materials under investigation from high Q resolution for phase transition analysis and large scale structure determination to high flux for measuring weak signals [19] It is thus optimally suited to study the in depth details of the evolution of a specific magnetic phase diagram under pressure.

An example of a multi-wavelength, quasi-Laue diffractometer is HFIR's IMAGINE, which is designed and optimized for the rapid collection of data at near-atomic resolutions (1.1 Å) from crystals with small volume (~0.1-1.0 mm^3) and large unit cell < 100 Å [20]. The white-beam

Laue capability provides a rapid and efficient survey of reciprocal space and enables measurement of many single-crystal diffraction spots simultaneoulsy. The cylindrical image-plate detector covers a full 360º, making excellent use of the wide-angle aperture available in the DAC.

The second polychromatic category includes SNS's time-of-flight (ToF) Laue diffractometers, which yield wavelength-resolved data (as wavelength can be extracted from ToF according to wavelength [Å]= 4000 * ToF [sec] / flight_path_length [m]). CORELLI is a third generation neutron diffractometer that combines the high-efficiency of ToF Laue diffraction to survey volumes of 3D reciprocal space with a statistical chopper for a cross-correlation method that reconstructs the elastic data from modulated data [21]. Its current detector configuration of ^{3}He tubes has large in-plane detector coverage (166º in total) and out of plane coverage (+/-28º). This makes it a very adaptable instrument to single-crystal studies in a diamond cell, since a large portion of the reciprocal space can be surveyed for small samples with their limited alignment options inherent to pressure work.

Finally, SNAP is ORNL's dedicated high pressure beamline, a highly versatile, high-flux, ToF diffractometer for medium resolution powder and potential high resolution single-crystal diffraction. A recent detector and software upgrade aims to bring its detector and software capabilities more in line with TOPAZ, the facility's general high resolution, chemistry diffractometer for single-crystal work. As a dedicated high pressure beamline, SNAPs key advantages lie in the fact that the high-flux beam is focused into a very small area, the detector positions adjust to cell orientations and its sample position is extremely accessible and accommodating of complex sample environments.

In terms of the science interest in their various high pressure single-crystal diffraction experiments, HB-3A and CORELLI typically focus on investigating solid state materials and past pressure cell studies on HB-3A as well as CORELLI have yielded full data for structure and magnetic structure refinement. In the few DAC studies, to date this has typically required thorough investigation of one or few representative individual magnetic peaks instead, for example, for their temperature dependence and to correlate with a magnetic phase diagram. IMAGINE, concentrating on supra- and macro-molecular compounds, is well suited to serve as a fast survey instrument providing a wide angular overview over a sample in a DAC prior to detailed studies of one or few peaks at other instruments. Considering the recent software and detector improvements of SNAP, we envision collecting high pressure single-crystal data for full structure refinement and quantitative analysis also on this instrument with commissioning in progress. Finally, work continues on all instruments to enable the collection of sufficient number of reflections and optimize correction procedures to enable full refinement in the DAC**.**

3. Cell description

The DAC consists of a cylinder with large scattering cutouts, two pistons with removable seats, an endcap, a spring and a spring retainer (see Fig. 1). The outer diameter of the cell at its widest

diameter (the spring retainer) is 50 mm and thus potentially suitable for ORNL's magnets. Together with the steep design for anvil and seat, the large cut-out allows for diffraction angles of ±60º. With the exception of the anvils and steel gasket, all cell parts are made from CuBe (alloy 25, TH04 temper) for its non-magnetic properties and superior cooling characteristics. Furthermore, for this design the pistons have been encased in an acetal resin to minimize friction upon cooling (which has caused seizing in the past).

In contrast to the previous wide-angle design [18], the size of the spring has been increased in thickness and diameter to optimize strength and deflection path-length. The spring material has been altered to CuBe, which has inferior mechanical properties compared to the past steel. Nonetheless, testing of the spring demonstrated that minimal plastic deformation commenced at a nominal 9 tons applied in a Carver press with deformation noticeable upon a nominal 10 tons. Load applied with this type of spring is significantly more reproducible than stacks of Belleville (conical spring) washers due to the absence of friction.

Moreover, the past cell design consisted of one single metal piston into which the anvil was incorporated. Upon anvil fracture, the anvil could often not be removed. This issue has been overcome through a removable seat with a hole in the back. This allows now for easy anvil replacement.

Furthermore, the design of the Versimax® anvils has been improved since the previous cylindrical shape often resulted in median cracking at very low loads (~2 tons). While such cracked anvils could still be taken to high pressures, they typically fully shattered at loads of ~8 tons and could not be recovered. Therefore, the current design includes now a conical bottom support as previously used for single-crystal CVD anvils in membrane-driven SNAP DACs [17]. In a failure test, this design was taken successfully to over 10 tons upon which one anvil shattered due to gasket and seat failure/yielding. Several experiments to 8 and even 10 tons applied load have not resulted in any anvil fracture. This is at par or even superior to single-crystal anvils. It is also highly noteworthy that the anvils are significantly tougher than single-crystal anvils which makes preparation and alignment of a cell an easier and faster undertaking.

Another key advantage of these Versimax® anvils over single-crystal anvils lies in the fact that larger samples are possible due to their increased surface roughness and friction with a gasket material. For large single-crystal anvils the ideal thickness of a gasket corresponds to ~10% of culet diameter. For larger thickness, friction between the anvils upon pressure increase is not sufficient and as a result the gasket hole expands upon pressure increase rather than shrink which limits the pressure than can be applied. In the case of the Versimax® anvils, however, the friction properties are superior and a gasket thickness above ~10% can be used. Thus, for a 3mm culet anvil, the gasket hole is typically 0.3-0.35mm high for single-crystal anvils but 0.5mm for Versimax®. These 30-40% higher gasket hole also translates to a 30-40% higher sample.

The performance of the cell was tested through offline compression, equipped with two 6 mm CVD anvils (in steel seats) rather than with Versimax® anvils. The CVD anvils culets were polished to ø 2 mm, and a gasket was prepared from a polished 301 stainless steel disk (ø 2 mm)

and a 6 mm O.D. 15-5 PH alloy belt. The cell was loaded with ruby as a manometer and KCl, chosen for its high compressibility. Load was applied in 1 ton steps in a Carver press and locked in. Pressure was determined from the ruby fluorescence [22]. At the maximum load of 7 tons, a pressure ~18.5 GPa was reached, the record pressure for such a clamped DAC to date. The resulting pressure-load curve compared to previous curves taken from [17,18] is shown in Fig. 2.

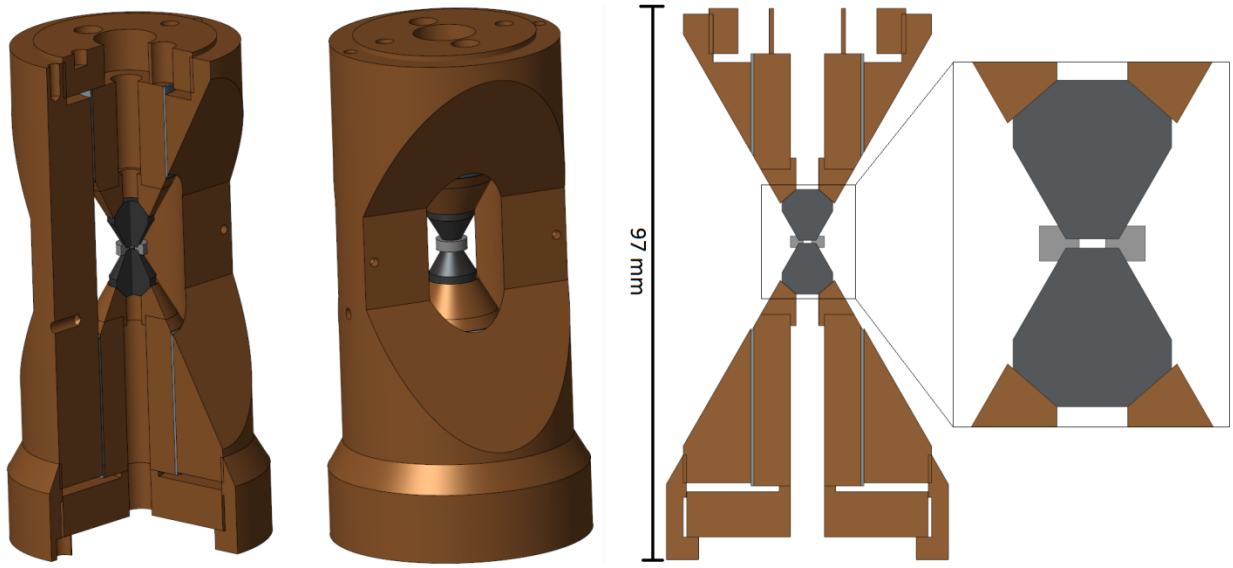

Figure 1: *Scaled-down 3D CAD rendering of the wide-angle CuBe diamond cell. Key features include the large scattering apertures of 120°, the conical Versimax® anvils and the large CuBe spring used to lock in pressure at room and also low temperature. Anvils and gasket are highlighted in a zoom in.*

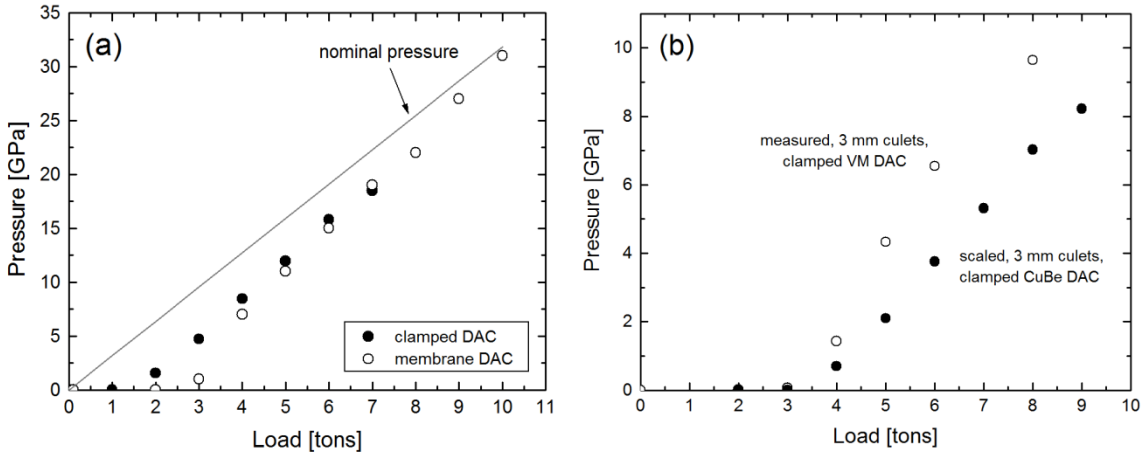

Figure 2: *Pressure-load curve measured via ruby fluorescence in the clamped CuBe DAC compared to previous pressure-load curves. (a) The pressure-load curve measured in the clamped DAC compared to one measured online using the membrane set-up [17]. 6 mm CVD anvils with 2 mm culets were used in both cases. Nominal pressure is force over area. (b) The pressure-load curve taken from a clamped DAC (maraging steel) with Versimax® anvils (ø 3 mm culets) [18] compared to the curve measured here scaled to 3 mm culet sizes.*

geometry were used. In contrast, scaling the pressure-load curve to 3 mm culet size does not replicate a previous pressure-load curve obtained from a clamped steel DAC with 3 mm culet Versimax® anvils [Fig2(b)]. While the gasket geometry had been the same in both cases, the anvil geometry was not. Namely, an 82º included angle was used for the CVD anvils but a steep 60º angle was used for the Versimax®. Such a steeper angle is expected to result in faster pressure increase (i.e. a steeper pressure-load curve), as we do indeed observe here. It thus appears clear that the anvil geometry governs these pressure-load curves more critically than the exact cell design in this family of neutron DACs. Nonetheless, the new spring effectively clamps in pressure and produces pressure-load curves comparable to previous cells.

Cell and anvil arrangement is now straightforward to prepare and use. It boasts a simple standardized design and anvil/gasket set-up that makes it in use and preparation more akin to a clamp cell or Paris-Edinburgh cell rather than a single-crystal DAC. The maintenance of this cell will therefore be transferred to the centralized Sample Environment group and the cell will be available in the general user program on several beamlines. This is an important step in the deployment of neutron DACs as the use of past cells always relied on a small, dedicated team.

4. Scientific examples

Many experiments on high pressure single-crystal diffraction in the DAC at SNS and HFIR focusses on the study of magnetic phase diagrams. To date these studies have typically assessed one or a few representative magnetic diffraction peak in great depth across the temperature regime down to 5 K currently. Future development would prefer to see even lower temperatures coupled with high magnetic fields. Two examples are briefly detailed for SNS's CORELLI and HFIR's HB-3A beamlines.

MnP is an ideal test sample for the DAC for single-crystal diffraction due to its well-characterized pressure-temperature phase diagram. Our previous measurements using the palm cubic anvil cell have detailed the magnetic moments and transition temperatures under different pressures [6,23,24]. This makes MnP an ideal prototype magnetic system to characterize new pressure cells as we have indeed demonstrated previously for a DAC with a solid pressure medium [18]. For the present experiment, a MnP crystal of 0.92 x 0.4 x 0.2 mm^3 was loaded in the DAC (3mm culet Versimax® anvils, 15-5 PH pre-formed gasket, *ø* 1.5 mm x 0.5 mm *h* gasket chamber) together with deuterated glycerin as pressure medium. Thin disks of aluminum foil were placed on both anvils to create an encapsulated gasket. The cell was pressurized offline and measured at various pressures up to 8 GPa at CORELLI. Pressure was estimated from the pressure-load curves and confirmed based on the magnetic phase diagram. Figure 3(a–d) shows the intensity contour maps of neutron diffraction data measured at 6 K at the different pressures. At 1.4 GPa, the ferromagnetic (FM) state is observed at 6 K, while above 2 GPa, the helical-b magnetic phase is the ground state. A detailed temperature dependence of the magnetic intensity at 5.6 GPa is shown in Fig. 3(e). Note that the 8 GPa measurement is not shown as the sample

shattered at this point due to bridging with the top anvil. No effects of non-hydrostaticity were observed as will be addressed in more detail in the next section.

With increasing pressure, the magnetic moment decreases and the incommensurate position of the magnetic peak increases. These results agree well with the measurements performed in the palm cubic anvil cell [6,23,24]. The intensity of the magnetic peak of MnP provides a good estimation of the smallest magnetic moment that can be investigated. For 3 mm Versimax® anvils in the DAC, CORELLI is capable of measuring magnetic order with a moment as low as ~ 0.25 μB/Volume under high pressure.

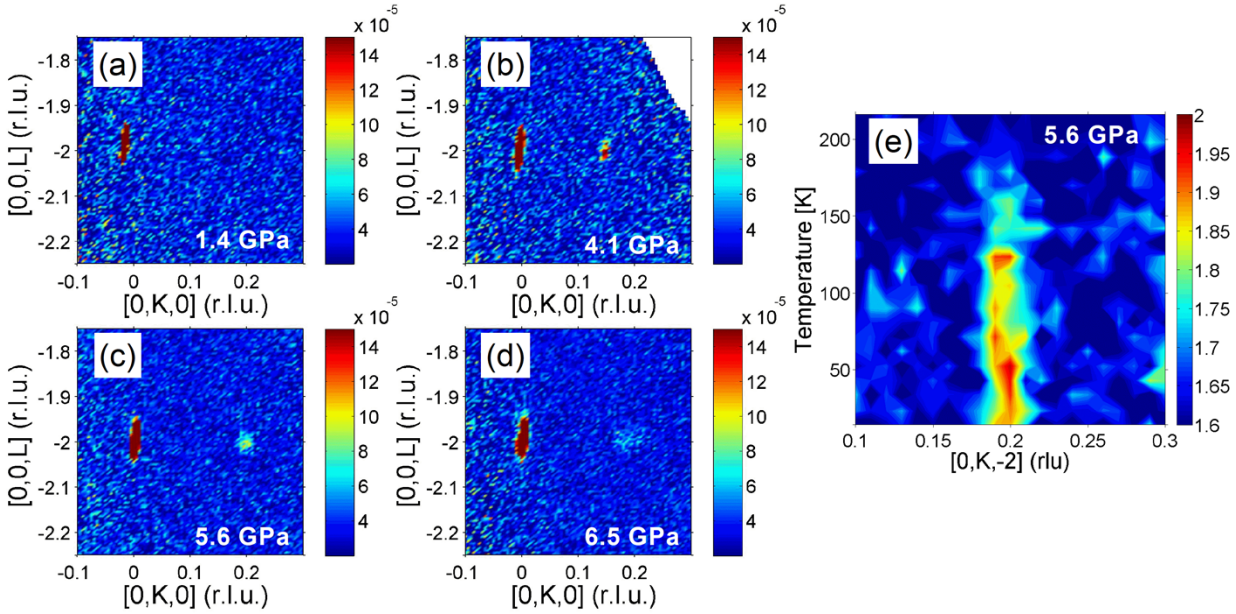

Figure 3: *Intensity contour maps of neutron diffraction of MnP in the DAC at 6 K in the (0KL) scattering plane measured at CORELLI at (a) 1.4 GPa (FM phase), (b) 4.1 GPa (helical-b phase) (c) 5.6 GPa (helical-b phase) (d) 6.5 GPa (c) 5.6 GPa (helical-b phase) and (e) Temperature dependence of the (0,**δ**,-2) magnetic peak measured at 5.6 GPa.*

Another example of such a magnetic system of interest is a hexaferrite such as $Ba_{0.4}Sr_{1.6}Mg_2Fe_{12}O_{22}$ (lattice parameter $a = b = 5.847$ Å, $c = 43.356$ Å, space group $R\bar{3}m$). For this material a recent new record for the magnetoelectric coefficient in a single-phase material has been established through systematically tuning the ground state spin cone symmetry by systemically doping Sr on the Ba site [25]. The DAC was employed to further study the effects of pressure (as substitute of chemical pressure) for the underlying mechanism. Here, we thus prepared a CuBe SNAP DAC with ±35º opening angle [17] for an experiment on HB-3A with Versimax® anvils (ø 3 mm culets), a 15-5 PH pre-machined gasket and an endcap modified to act as spring. A crystal with dimensions of 0.9 x 0.9 x 0.15 mm^3 was surrounded with Pb inside the gasket chamber (1.5 mm diameter, 0.5 mm height).

The pressure, that was applied offline and locked-in, was estimated from an extrapolation of an equation of state (EoS) obtained in a conventional clamp cell on the sample material up to 1.8 tons (3rd order Birch-Murnaghan, fitted B_0 = 86 GPa, set B'_0 = 4 GPa). The resulting pressure shift of the (003) nuclear peak at room temperature is shown in Fig. 3(a). Clearly, the peak here starts broadening at ~ 2 GPa and very significantly at pressures above 4 GPa (which even has the trend of splitting at 4.7 GPa). This prevented the extraction of reliable information on the pressure induced effect regarding the crystal structure and magnetic phase of the sample. Further experiments using single crystal CVD anvils (ø 2 mm culets) and hydrostatic pressure media such as glycerin and gas pressure media are currently in progress.

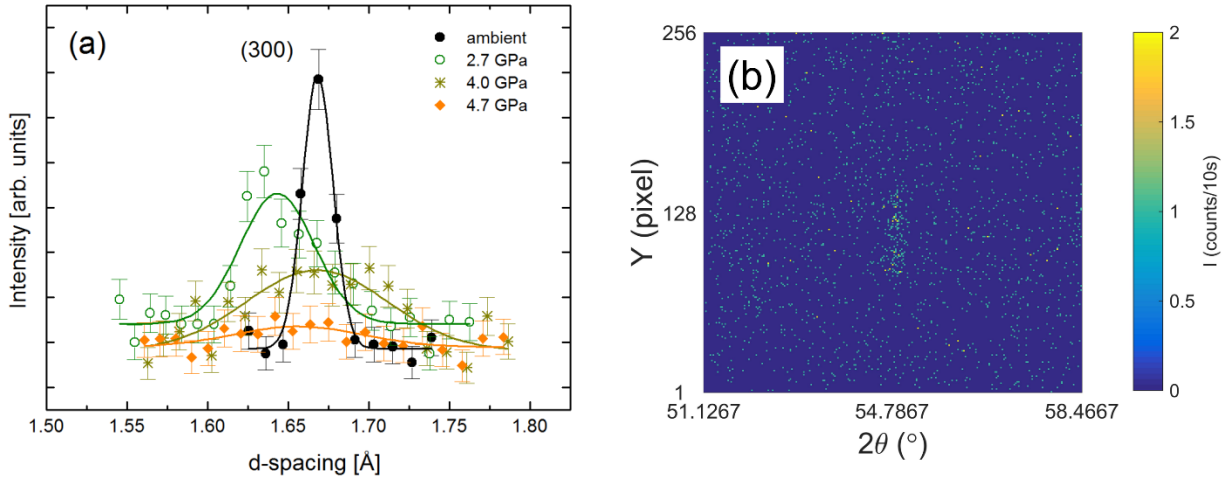

Figure 4: *Room temperature data from hexaferrite measured on HB-3A loaded in the DAC with lead as pressure medium. (a) Evolution of the (300) nuclear peak with pressure (b) Example of the (300) nuclear peak with λ = 1.546 Å as seen on HB-3A.*

5. Pressure transmitting media

Quite clearly, the choice of pressure transmitting medium is the key critical issue for the study of single crystals under pressure. Gas pressure media provide the best hydrostaticity available for use with single-crystal anvils. However, Versimax® anvils prevent the use of gases due to inherent porosity of the polycrystalline diamond coupled with poor adhesion of any material deposited on the anvil that could counteract the porosity. They do however, exhibit the unique advantage over single-crystal anvils that samples may be up to 30-40% taller, a rather important factor for neutron diffraction studies where sample size is often the limitation. Thus, the pressure transmitting medium was optimized for Versimax® anvils and several solid and liquid pressure media were tested.

In the past study with Versimax® anvils on CORELLI, we employed solid KBr, which was sufficiently hydrostatic to 2 GPa and lead, which appeared comparable to KBr to higher

pressures of up to 7.5 GPa [18]. Based on the HB-3A data presented above however, the peak broadens significantly above ~2 GPa.

A better alternative are liquid pressure-transmitting media. Therefore, we loaded 4:1 methanol:ethanol (which is hydrostatic to at least 10 GPa) after placing a thin 3 mm diameter Al foil below and above the gasket, i.e. with the aim to create a form of an encapsulated gasket. This, however, was not successful since the methanol:ethanol had always escaped upon inspection of gasket/sample recovered from pressure.

In the past, (deuterated) glycerin has been reported as a very good alternative [5,26-28]. It exhibits low compressibility, small volume contraction upon cooling and hydrostaticity up to at least ~7 GPa (see [5] and refs therein). To evaluate this for neutron single-crystal diffraction, three data sets from CORELLI and HB-3A were evaluated, (i) the past CORELLI data on MnP loaded with KBr [18], (ii) the CORELLI data on MnP loaded with glycerin presented above, and (iii) the HB-3A data on hexaferrite loaded with lead shown above. To quantify the (non-) hydrostaticity, the nuclear peaks from the different loadings were fitted with Gaussians using the package Origin. The resulting peak widths versus pressure from all experiments are shown in Fig. 4, whereby the width normalized to d-spacing of the reflection is shown in (a) and relative to the starting width of the respective peak in (b).

At lower pressures, the peak width is lower for the HB-3A data due to HB-3A's better Q-resolution. Upon pressure increase, the relative width increases exponentially in the Pb and KBr experiments above ~2 GPa, while it remains constant in the glycerin experiment on CORELLI.

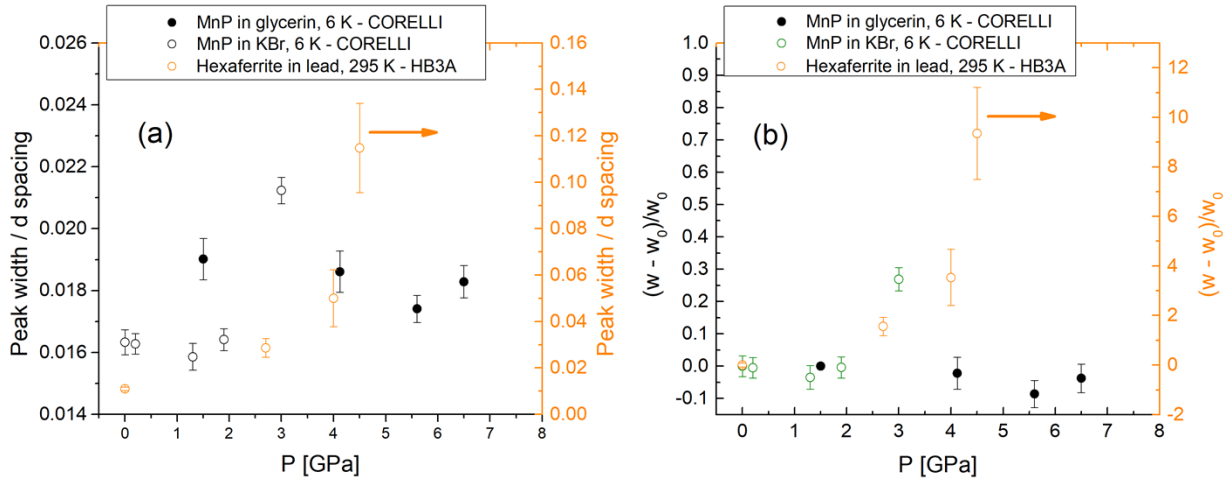

Figure 5: *Data on the peak width versus pressure extracted from four different experiments, MnP measured on CORELLI in KBr [18] and glycerin and hexaferrite measured on HB-3A in lead (a) Peak width normalized against d-spacing of respective peak. (b) Peak width relative to starting width w_0 at ambient pressure. Note the different scale (on right) for hexaferrite in lead in both plots.*

Clearly, this result from CORELLI as well as past reports indicate that deuterated glycerin is a promising pressure transmitting medium for neutron scattering. Indeed, it has been assessed extensively for its hydrostaticity in diamond cells [26-28]. In these past studies rubies were only placed within the inner two-thirds or even the very center of gasket chamber only. Furthermore, details were given on the *pressure variation* across the gasket chamber, but not so much on the shear *pressure gradient* itself. As our neutron studies require very large culet sizes and thus a low gradient across a very large region and height, glycerin's hydrostaticity to 10 GPa was further evaluated.

A Boehler plate DAC [3] (*ø* 400 µm culet, 301 FH steel gasket, *ø* 180 µm x 50 µm *h* gasket chamber) was loaded with a drop of glycerin mixed with rubies. This ensured that the rubies did not all touch the diamond surface, rather some were fully surrounded by glycerin. The fluorescence of seven rubies aligned from center to edge of gasket [see Fig. 5(a)] were systematically measured up to a pressure of ~13 GPa. This allowed to measure the pressure variation and pressure gradient across the entire gasket width as well as height. As Klotz *et al.* [28] before, the standard deviation σ of the individual pressures P_i indicated by the N ruby spheres was used to estimate the pressure variation of glycerin:

$$\sigma = \sqrt{\frac{1}{N}\sum_{1}^{N}(P_i - \overline{P})^2}$$

where $\overline{P}$ is the average pressure of the N ruby spheres. The individual pressures P_{i} of each ruby were thereby calculated relative to the starting value of the respective ruby.

The resulting deviation σ with average pressure increase is shown in Fig. 4(b). The positions of the R1 and R2 ruby peaks and their corresponding widths were determined by fitting with two Lorentzian functions. We also compared the average change in width $\Delta\,\Gamma$ of the R1 line and average change in R1-R2 separation $\Delta\,\mathrm{R1}-\mathrm{R2}$ and $\Delta\,\Gamma$ of the R1 compared to ambient pressure are shown as insets Figure 4(b).

The standard deviation remains relatively flat even through the glass transition at 5.5 GPa. Upon compression to above ~9 GP, significant increase in the deviation is observed, a higher pressure than comparable studies that observed this increase upon the glass transition [28]. The exact origin of these differences is unknown but may be due to slight differences in methodology.

Finally, the maximum pressure difference measured across all rubies versus the average pressure is shown in Fig. 4(c). Until ~8 GPa, the variation was statistical with no pattern discernable and not repeatable from one pressure point to the next. The variation may be attributed to slight difference in laser focusing as the rubies are not all placed on the culet surface but mixed through the glycerin. From 10 GPa onward, a typical Hertzian gradient following is observed. The increasing gradient is given in the figure. The absence of a clear gradient below 10 GPa quite strongly suggests sufficient hydrostaticity below this pressure.

The CORELLI experiment was performed to a maximum pressure of $P = 6.5$ GPa and conditions proved sufficiently hydrostatic. Based on the ruby data, this level of hydrostaticity remains constant close to 10 GPa as suggested by the relatively flat standard deviation σ and even more importantly the absence of a shear pressure gradient to above 10 GPa. It is thus expected that conditions remain sufficiently hydrostatic for single-crystal diffraction to a pressure of ~9-10 GPa, even higher than expected from past reports.

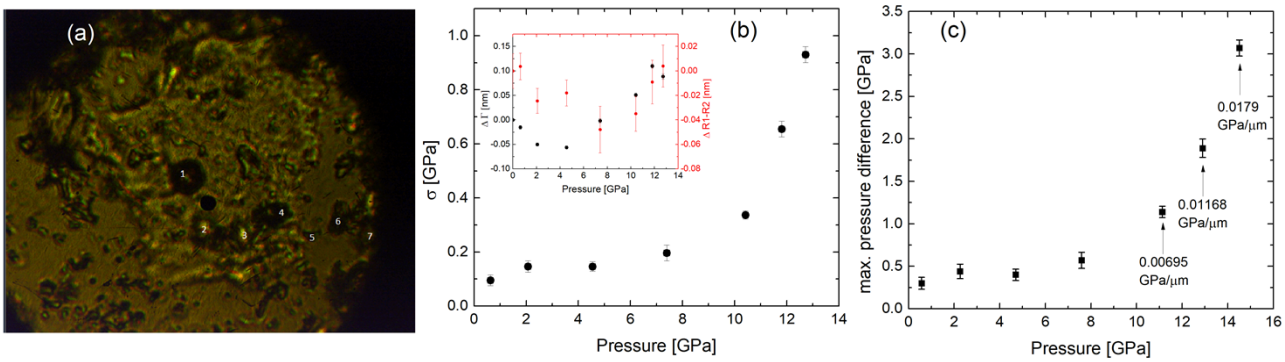

Figure 6: *(a) Optical image of the rubies in the diamond cell taken on the SNAP Raman stand. The rubies used for evaluation are numbered 1–7. The center hole is the entrance to the spectrometer and thus defines the spatial resolution of the measurement. (b) The standard deviation σ with increasing average pressure obtained from these rubies. The pressure-dependence of the average $\Delta\Gamma$ and average Δ R1-R2 are shown as inset. (c) Maximum pressure difference from the rubies placed across the culet. The typical gradient observed from ~10 GPa onward is indicated.*

6. Developments and directions

With the present work, a neutron diamond cell optimized for single-crystal diffraction and easy use across several beamlines has been demonstrated. With 60º Versimax® anvils and glycerin, it can operate under sufficiently hydrostatic conditions close to ~10 GPa on a single crystal of ~0.7 x 0.7 x 0.2 mm^3 size. Here, we will now show an implementation of this cell on HFIR's IMAGINE and a further feasibility test on SNS's SNAP.

6.1 The diamond cell on IMAGINE

The development of single-crystal diffraction in a diamond cell aims to take advantage of the large coverage and high throughput capabilities of HFIR's Laue diffractometer IMAGINE. This instrument is optimized for wavelengths above $\lambda = 2$ Å which, incidentally, excludes the majority of scatter from steel gasket and Versimax® anvils. Furthermore, IMAGINE is equipped with elliptically focusing mirrors that concentrate the beam to 3.2 x 2.0 mm^2 at the sample (increasing the flux density more than 20-fold). This limits the incident beam to predominantly gasket and sample only, thus obviating the need for further collimation or masking.

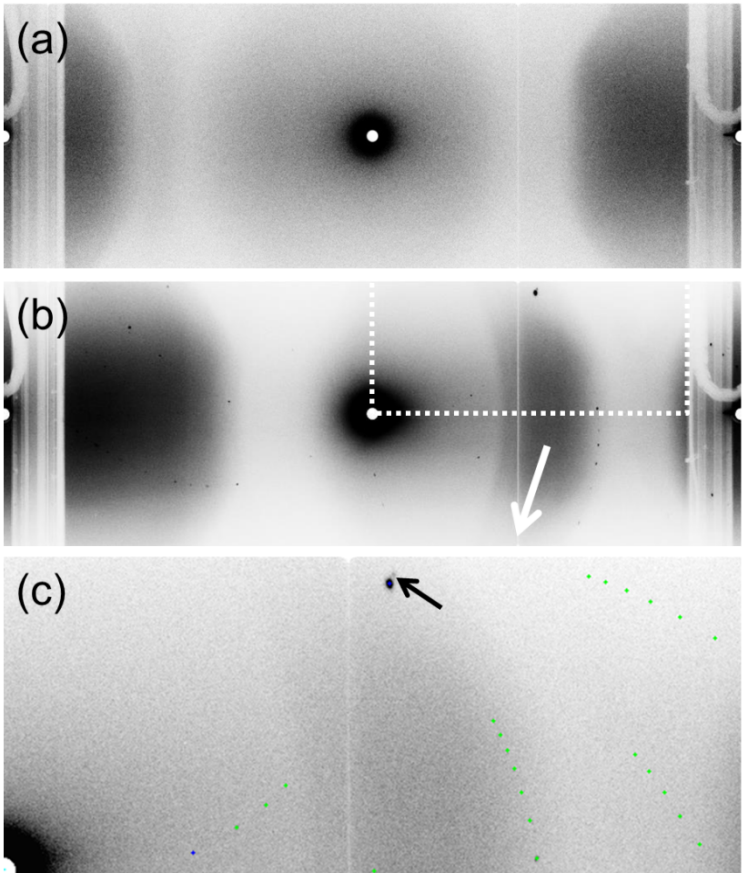

Figure 7: *(a) Relatively low background from empty cell without any parasitic single-crystal peaks. Note that the background scatter is predominantly due to backscatter of the steel gasket. (b) Diffraction from a hexaferrite crystal measured inside in the DAC rotated to 45°. (c) Simulated diffraction pattern superimposed on a zoomed-in region [indicated in (b)] of the experimental data. The magnetic super-lattice is evident as satellite peaks on the nuclear peaks and one such example is indicated by an arrow.*

The DAC was loaded into IMAGINE and assessed for background. No parasitic single-crystal peaks are visible (see Fig. 5(a)) although significant shadowing from the diamond cell itself is evident. A hexaferrite sample of the same nature and dimensions as above was loaded into the DAC (*ø* 3 mm culet Versimax® anvils, pre-machined 15-5 PH gasket, *ø* 1.5 mm x 0.5 mm *h* gasket hole). A reference quasi-Laue data set had been collected at 440K on IMAGINE on a larger crystal (not shown). This reference set provided data that extend out to 1.1 Å resolution. The wavelength range for the reference data set was 2.0 - 3.2A. The data set comprised 1826 measured reflections, of which 42 were higher harmonic superimposed reflections and the remaining were single reflections. The diffraction pattern from the crystal in the DAC resulting from a 1 hour exposure at a 45º rotation is shown in Fig. 5(b). In this geometry, at least 47 reflections were visible out to the same resolution. More reflections are likely to appear upon longer exposure times and/or addition of further rotations. Nonetheless, these proved sufficient diffraction spots to allow for indexing of the Laue diffraction pattern. Laue data frames were

measured, indexed and integrated using the LAUEGEN suite of programs, modified to account for the cylindrical geometry of the detector [29,30]. Once reduced and wavelength-normalized, data can be analyzed using standard crystallographic structure refinement and visualization packages.

An example of an indexed region zoomed-in for clarity is shown in Fig 5(c). Thereby, the indexing successfully predicted the nuclear peaks. Furthermore, evidence for the magnetic superlattice of the sample is also visible as the smaller satellite spots slightly dislocated from the nuclear spots (as indicated in the black arrow position for an example).

6.2 Single-crystal diffraction on SNAP

The current development equally aims to take advantage of the high flux of the dedicated high pressure beamline SNAP and its highly pixelated detectors. In contrast to all other instruments/experiments described here, the typical sample/beam geometry on SNAP allows for a beam direction coaligned with the compression axis in addition to the perpendicular axis. That is, while the beam enters through the gasket on other instruments it enters through the diamonds on SNAP in its typical arrangement for powder diffraction. With appropriate selection of incident beam collimation, this geometry often yields data free from gasket scatter. Specifically, the diamond reflections can be excluded in the reduction software MANTiD [31] from the data through a careful, non-automated indexing and masking procedure. Further careful corrections for diamond attenuation as detailed by Guthrie *et al.* [32] are then required. This conventional orientation on SNAP (i.e. along the compression axis) has however, one further critical drawback for single-crystal diffraction: there are very few alignment possibilities – only rotation about the beam – and desired reciprocal space might be inaccessible.

Therefore, use of the vertical orientation (i.e. beam perpendicular through the gasket) as on the other beamlines is also advantageous as it allows for free vertical rotations. In this geometry, it is possible to collect multiple datasets at different rotations to increase reciprocal space coverage. Moreover, the beam on the sample does not suffer the adverse effects of wavelength-dependent truncation that occurs when entering through the diamonds [32] although diamond scatter is still observed. Finally, this geometry allows for tilt of the cell out of the vertical, which can simplify sample alignment significantly.

To evaluate these conditions, ToF diffraction data were collected in both configurations on a single crystal of KD_2PO_4 (KDP), an ideal test material [33-36]. KDP (lattice parameter $a = b =$ 7.4794 Å, c = 6.995 Å, space group $I\bar{4}2d$, crystal dimension of 0.84 x 0.46 x 0.21 mm^3) was loaded into a typically configured SNAP DAC (ø 6 mm single-crystal CVD anvils, ø 2 mm culets, indented T301 gasket, ø 1 mm hole). Note that this configuration was used for test purposes. A larger culet and gasket would be required for an experiment on this crystal. The SNS data-reduction software suite MANTiD was used for data processing.

Resulting ToF diffraction data, unprocessed on the detector, indexed on the detector and integrated to 1D-profile are shown in Figure 6. Data obtained in the perpendicular direction (i.e. beam through the diamonds) are shown in the left column and data obtained in the normal direction (i.e. beam through gasket) in the right column. Note that the *d*-spacing range for the unprocessed ToF data shown in Fig. 6(a) and (b) was reduced to 1.12-1.98 Å in order to highlight diffraction spots. Only data from one of the two detector banks are shown for simplicity. Such obtained ToF data are surveyed to identify candidates for sample peaks and superimposed with a set of predicted sample peaks. Currently, this is a somewhat tedious and manual operation that is in the process of being automated. As shown in Fig. 6(c) it is possible to find 338 peaks in a single orientation for data analysis under the perpendicular orientation. Although the data in the normal configuration show very strong steel peaks, indexing of the KDP crystal was still possible as shown in Fig. 6(d). In this configuration, fewer reflections are predicted (262 out of 2074 allowed). Reduction of both data sets to a 1D profile is then shown in Fig 6(e) and (f) with diamond and steel peaks indicated. Clearly, the beam-through-diamond orientation provides the unique advantage that gasket scatter can potentially be excluded. Due to the possibility of sample/cell rotation, the beam-through-gasket direction may however, also be advantageous on SNAP.

7. Conclusions

Here, we have demonstrated a highly user-friendly and easily maintainable diamond cell optimized for hydrostatic single-crystal diffraction to ~9-10 GPa at several beamlines across SNS and HFIR. The use of inexpensive, high-friction Versimax® in a conical design together with highly viscous glycerin as pressure-transmitting medium allows for (sufficiently) hydrostatic conditions on very large samples up to ~9-10 GPa. The current seat/anvil set-up allows for easy alignment and replaceability of anvils. A similar spring design, but now also made from CuBe, as was used in the past [14] allows for offline pressurization and easy portability of the cell. For the first time, large single-crystal CVD anvils were used with such a clamp DAC, and pressures close to 20 GPa were achieved. The use of the cell for single-crystal studies was successfully demonstrated across SNS's SNAP and CORELLI beamlines as well as HFIR's HB-3A and IMAGINE beamlines. This clearly highlights the versatility of this DAC design. Finally, the cell is made entirely of non-magnetic CuBe and is of sufficiently small diameter to become compatible with existing magnets at ORNL, thereby opening the possibility of future studies exploring quantum phenomena under the combined extreme conditions of high pressure, ultra-low temperature and high magnetic field.

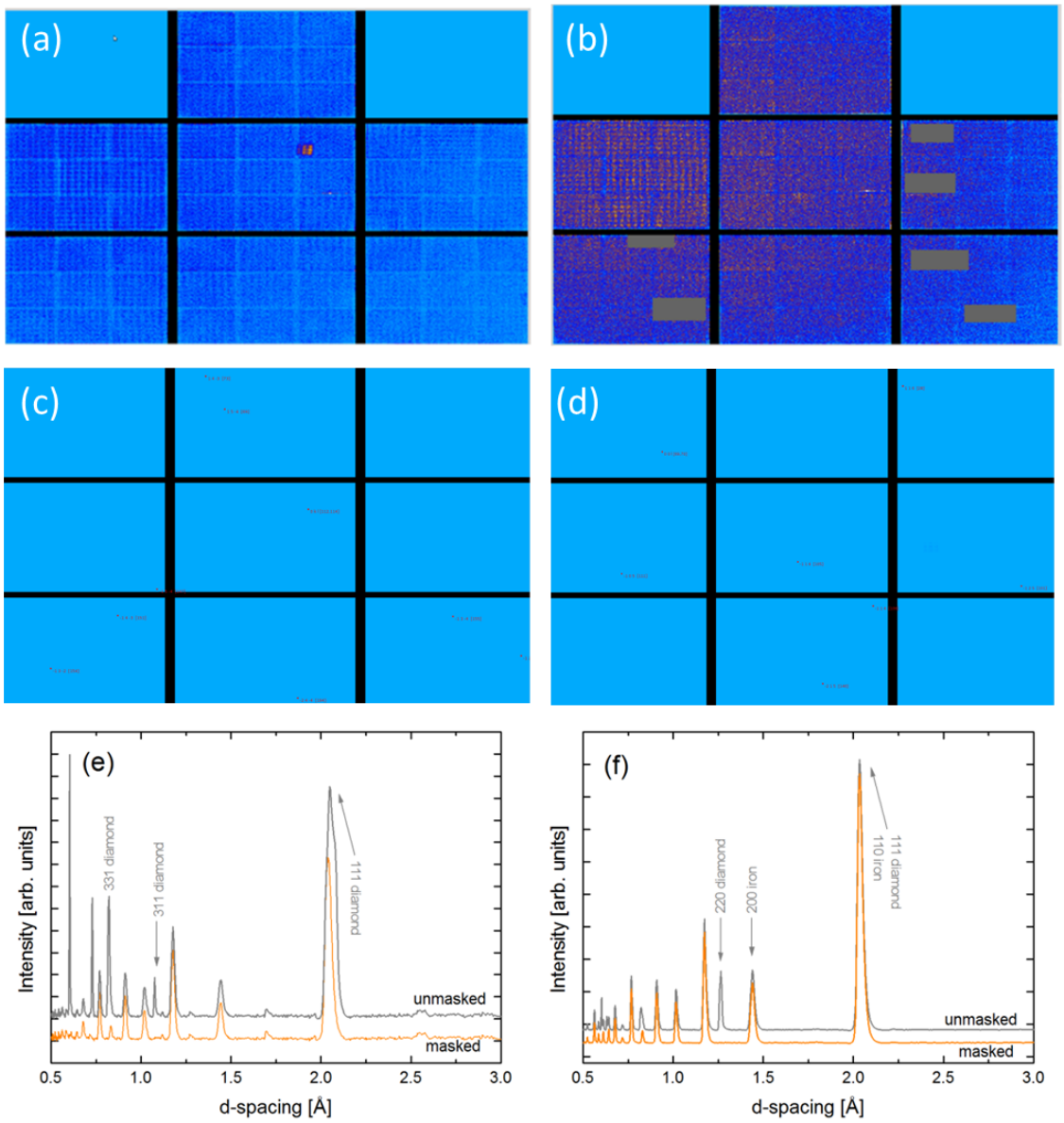

Figure 8: *Single-crystal diffraction data from a KDP crystal in a DAC on SNAP in two different DAC orientations. (a) Unprocessed ToF diffraction data as collected on the East detector depicted in a reduced d-range from 1.12-1.98 Å in an orientation where the beam entered through the diamond and (b) unprocessed ToF diffraction data depicted in the same manner in an orientation where the beam entered through the gasket. (c), (d) Indexed single-crystal diffraction from the two data sets shown above. (e), (f) Diffraction ToF data converted to d-spacing and reduced to a 1D profile from East and West detectors for both cases. Examples of diamond and steel (iron) peaks are indicated. The unmasked 1D profile (grey) is thereby compared to the 1D profile with the single crystal diamond peaks masked and subsequently removed (orange).*

Acknowledgment

The authors gratefully acknowledge Young Sun (Institute of Physics, Chinese Academy of Sciences, China) for the hexaferrite crystals. Equally, the authors gratefully acknowledge Luke L. Daemen (Oak Ridge National Laboratory) for the preparation of the KDP crystal. This work was conducted at the SNAP and CORELLI beamlines of the Spallation Neutron Source and the HB3A and IMAGINE beamlines of the High Flux Isotope Reactor, both DoE Office of Science User Facilities operated by Oak Ridge National Laboratory. This study was supported in part by the U.S.-Japan Cooperative Program on Neutron Scattering. Work by RB was supported by the Energy Frontier Research in Extreme Environments (EFree) Center, an Energy Frontier Research Center funded by the U.S. Department of Energy (DOE), Office of Science, Basic Energy Sciences (BES) under award number DE-SC0001057.

References:

[1] H-K. Mao, X.-J. Chen, Y. Ding, B. Li, and L. Wang, Rev. Mod. Phys. 90, 015007 (2018).

[2] G. Shen and H.-K. Mao, Rep. Prog. Phys. 80 016101 (2017).

[3] R. Boehler, Review of Scientific Instruments 77, 115103 (2006).

[4] I. Kantor, V. Prakapenka, A. Kantor, P. Dera, A. Kurnosov, S. Sinogeikin, N. Dubrovinskaia, and L. Dubrovinsky, Review of Scientific Instruments 83, 125102 (2012).

[5] S. Klotz, "Techniques in high pressure neutron scattering", CRC Press, Taylor & Francis Group (Boca Rota, USA), 2013.

[6] S. E. Dissanayake, M. Matsuda, K. Munakata, H. Kagi, J. Gochi, and Y. Uwatoko (Submitted to *J. Phys.: Conf. Ser.*)

[7] H. Ahsbahs, Revue Phys. Appl. 19, 819-821 (1984).

[8] W.F. Kuhs, H. Ahsbahs, D. Londono, J.L. Finnley, Physica B 156 & 157, 684-687 (1989).

[9] T. Osakabe, K. Kuwahara, D. Kawana, K. Iwasa, D. Kikuchi, Y. Aoki, M. Kohgi, H. Sato, Journal of the Physical Society of Japan 9, No. 3, 034711 (2010).

[10] G. J. McIntyre, L. Mélési, M. Guthrie, C. A. Tulk, J. Xu and J. B. Parise, J. Phys.: Condens. Matter 17 S3017–S3024 (2005).

[11] I. N. Goncharenko, High Pressure Research, 24:1, 193-204 (2004).

[12] V.P.Glazkov, I.N.Goncharenko, A.I.Irodova, V.A.Somenkov, S.Sh.Shilstein, S.P.Besedin, I.N.Makarenko, S.M.Stishov, Z.Phys. Chem. 163, 509 (1989).

[13] I.N. Goncharenko, P. Loubeyre, Nature 435, 1206–1209 (2005).

[14] J. Binns, K.V. Kamenev, G.J. McIntyre, S.A. Moggach, S. Parsons, IUCrJ 3, 168-179 (2016).

[15] Andrzej Grzechnik, Martin Meven, and Karen Friese, J. Appl. Cryst. 51 (2018). doi.org/10.1107/S1600576718000997

[16] R. Boehler, M. Guthrie, J.J. Molaison, A.M. dos Santos, S. Sinogeikin, S. Machida, N. Pradhan and C.A. Tulk, High Pressure Research, 33:3, 546-554 (2013).

[17] R. Boehler, J.J. Molaison, B. Haberl, Review of Scientific Instruments **88**, 083905 (2017).

[18] B. Haberl, S. Dissanayake, F. Ye, L. L. Daemen,Y.-q.Cheng, C. W. Li, A.-J. Ramirez-Cuesta, M. Matsuda, J. J. Molaison and R.Boehler, High Pressure Research 37, 495-506 (2017).

[19] Chakoumakos B.C., Cao H.B., Ye F., Stoica A.D., Popovici M., Sundaram M., Zhou W., Hicks J.S., Lynn G.W., Riedel R.A., Journal of Applied Crystallography, 44, 655-658 (2011).

[20] F. Meilleur, P. Munshi, L. Robertson, A. D. Stoica, L. Crow, A. Kovalevsky, T. Koritsanszky, B. C. Chakoumakos, R. Blessing and D. A. A. Myles, Acta Crystallographica Section D - Biological Crystallography 69: p. 2157-2160 (2013).

[21] F. Ye, Y. Liu, R. Whitfield, R. Osborn, S. Rosenkranz, J. Appl. Crystallogr. 51, 315 (2018).

[22] H-k. Mao, J. Xu, P.M. Bell, J. Geophys. Res. 91, 4673 (1986).

[23] M. Matsuda, F. Ye, S.E. Dissanayake, J.G. Cheng, S. Chi, J. Ma, H.D. Zhou, J.Q. Yan, S. Kasamatsu, O. Sugino, T. Kato, K. Matsubayashi, T. Okada, and Y. Uwatoko, Phys. Rev. B 93, 100405 (2016).

[24] S. Dissanayake et.al. "Helical magnetic state in the vicinity of superconducting MnP", manuscript in preparation.

[25] K. Zhai, Y. Wu, Sh. P. Shen, W. Tian, H. B. Cao, Y. Sh. Chai, B. C. Chakoumakos, D. Shang, L. Q. Yan, F. W. Wang & Y. Sun, Nature Communications 8, 519(2017).

[26] T. Osakabe and K. Kakurai, *Jpn. J. Appl. Phys.* **47** 6544 (2008),

[27] N. Tateiwa and Y. Haga *J. Phys.: Conf. Ser.* 215, 012178 (2010).

[28] S. Klotz , K. Takemura , Th. Strassle and Th. Hansen J. Phys.: Condens. Matter 24 325103 (2012).

[29] J.R. Helliwell, J. Habash, D.W.J. Cruickshank, M.M. Harding, T.J. Greenhough, J.W. Campbell, I.J. Clifton, M. Elder, P.A. Machin, M.Z. Papiz, and S. Zurek, *J. Appl. Cryst.* **22**, 483-497 (1989).

[30] J.W. Campbell, Q. Hao, M.M. Harding, N.D. Nguti, and C.J. Wilkinson, *Appl. Cryst.* **31**, 496-502 (1998).

[31] O. Arnold, *et al.,* Nuclear Instruments and Methods in Physics Research Section A, Volume 764, 11 Pages 156-166 (2014). http://dx.doi.org/10.1016/j.nima.2014.07.029

[32] M. Guthrie, C.G. Pruteanu, M.E. Donnelly, J.J. Molaison, A.M. dos Santos, J.S. Loveday, R. Boehler, C.A. Tulk, Journal of Applied Crystallography, 50, 76-86 (2017).

[33] C. L. Bull, M. Guthrie, R. J. Nelmes, J. S. Loveday, K. Komatsu, H. Hamidov, M. J. Gutmann. High Pressure Research 29:4, pages 780-791 (2009).

[34] G. M. Meyer, R. J. Nelmes and Vettier Journal of Physics C: Solid State Physics, Volume 13, Number 21 (1980).

[35] R. J. Nelmes , M. I. McMahon , R. O. Piltz & N. G. Wright, Ferroelectrics 124, Issue 1 Pages 355-360 (1991).

[36] R. J. Nelmes, Z. Tun, W.F. Kuhs, Ferroelectrics 71, 125-141 (1987).

Figures

Figure 1: Scaled-down 3D CAD rendering of the wide-angle CuBe diamond cell. Key features include the large scattering apertures of 120°, the conical Versimax® anvils and the large CuBe spring used to lock in pressure at room and also low temperature. Anvils and gasket are highlighted in a zoom in.

Figure 2: Pressure-load curve measured via ruby fluorescence in the clamped CuBe DAC compared to previous pressure-load curves. (a) The pressure-load curve measured in the clamped DAC compared to one measured online using the membrane set-up [boehler2017]. 6 mm CVD anvils with 2 mm culets were used in both cases. Nominal pressure is force over area. (b) The pressure-load curve taken from a clamped DAC (maraging steel) with Versimax® anvils (ø 3 mm culets) [haberl2017] compared to the curve measured here scaled to 3 mm culet sizes.

Figure 3: Intensity contour maps of neutron diffraction of MnP in the DAC at 6 K in the (0KL) scattering plane measured at CORELLI at (a) 1.4 GPa (FM phase), (b) 4.1 GPa (helical-b phase) (c) 5.6 GPa (helical-b phase) (d) 6.5 GPa (c) 5.6 GPa (helical-b phase) and (e) Temperature dependence of the (0,$\boldsymbol{\delta}$,-2) magnetic peak measured at 5.6 GPa.

Figure 4: Room temperature data from hexaferrite measured on HB-3A loaded in the DAC with lead as pressure medium. (a) Evolution of the (300) nuclear peak with pressure (b) Example of the (300) nuclear peak with λ = 1.546 Å as seen on HB-3A.

Figure 5: Data on the peak width versus pressure extracted from four different experiments, MnP measured on CORELLI in KBr [18] and glycerin and hexaferrite measured on HB-3A in lead (a) Peak width normalized against d-spacing of respective peak. (b) Peak width relative to starting width w_0 at ambient pressure. Note the different scale (on right) for hexaferrite in lead in both plots.

Figure 6: (a) Optical image of the rubies in the diamond cell taken on the SNAP Raman stand. The rubies used for evaluation are numbered 1–7. The center hole is the entrance to the spectrometer and thus defines the spatial resolution of the measurement. (b) The standard deviation σ with increasing average pressure obtained from these rubies. The pressure-dependence of the average $\Delta\Gamma$ and average Δ R1-R2 are shown as inset. (c) Maximum pressure difference from the rubies placed across the culet. The typical gradient observed from ~10 GPa onward is indicated.

Figure 7: (a) Relatively low background from empty cell without any parasitic single-crystal peaks. Note that the background scatter is predominantly due to backscatter of the steel gasket. (b) Diffraction from a

hexaferrite crystal measured inside in the DAC rotated to 45º. (c) Simulated diffraction pattern superimposed on a zoomed-in region [indicated in (b)] of the experimental data. The magnetic super-lattice is evident as satellite peaks on the nuclear peaks and one such example is indicated by an arrow.

Figure 8: Single-crystal diffraction data from a KDP crystal in a DAC on SNAP in two different DAC orientations. (a) Unprocessed ToF diffraction data as collected on the East detector depicted in a reduced d-range from 1.12-1.98 Å in an orientation where the beam entered through the diamond and (b) unprocessed ToF diffraction data depicted in the same manner in an orientation where the beam entered through the gasket. (c), (d) Indexed single-crystal diffraction from the two data sets shown above. (e), (f) Diffraction ToF data converted to d-spacing and reduced to a 1D profile from East and West detectors for both cases. Examples of diamond and steel (iron) peaks are indicated. The unmasked 1D profile (grey) is thereby compared to the 1D profile with the single crystal diamond peaks masked and subsequently removed (orange).

Figure 1

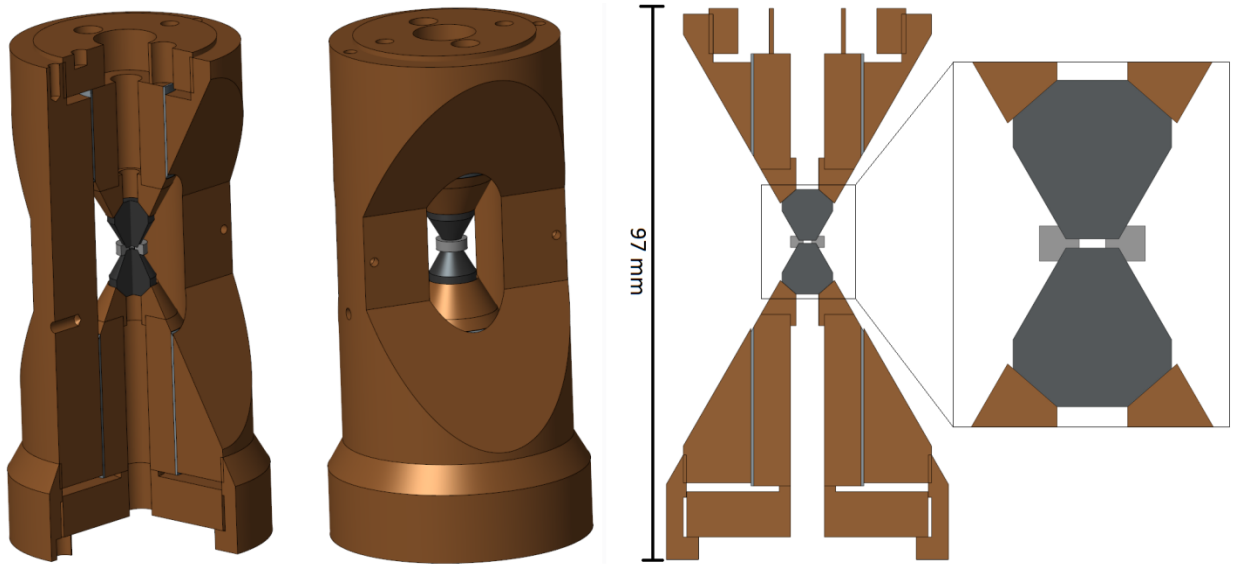

Figure 2

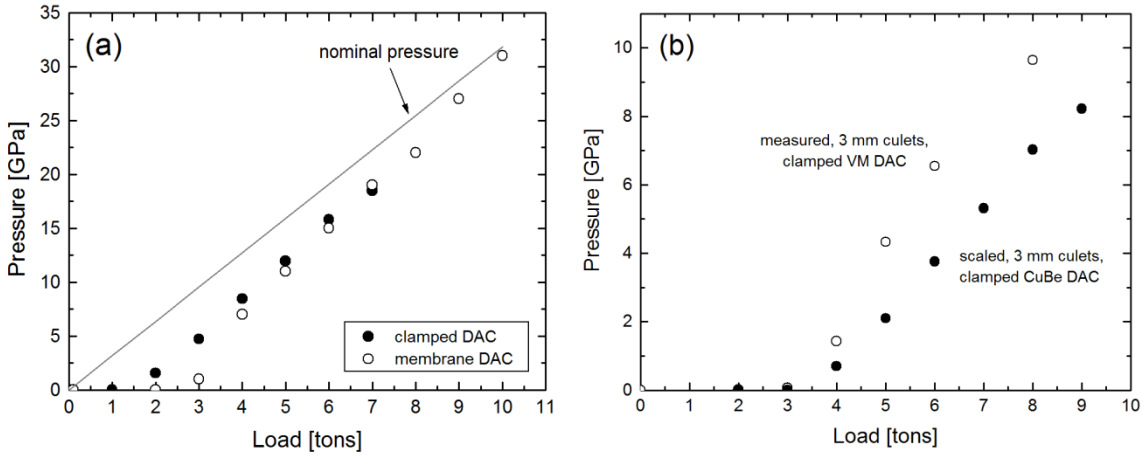
(a)
nominal pressure
clamped DAC
membrane DAC
Pressure [GPa]
Load [tons]
(b)
measured, 3 mm culets,
clamped VM DAC
scaled, 3 mm culets,
clamped CuBe DAC
Pressure [GPa]
Load [tons]

Figure 3

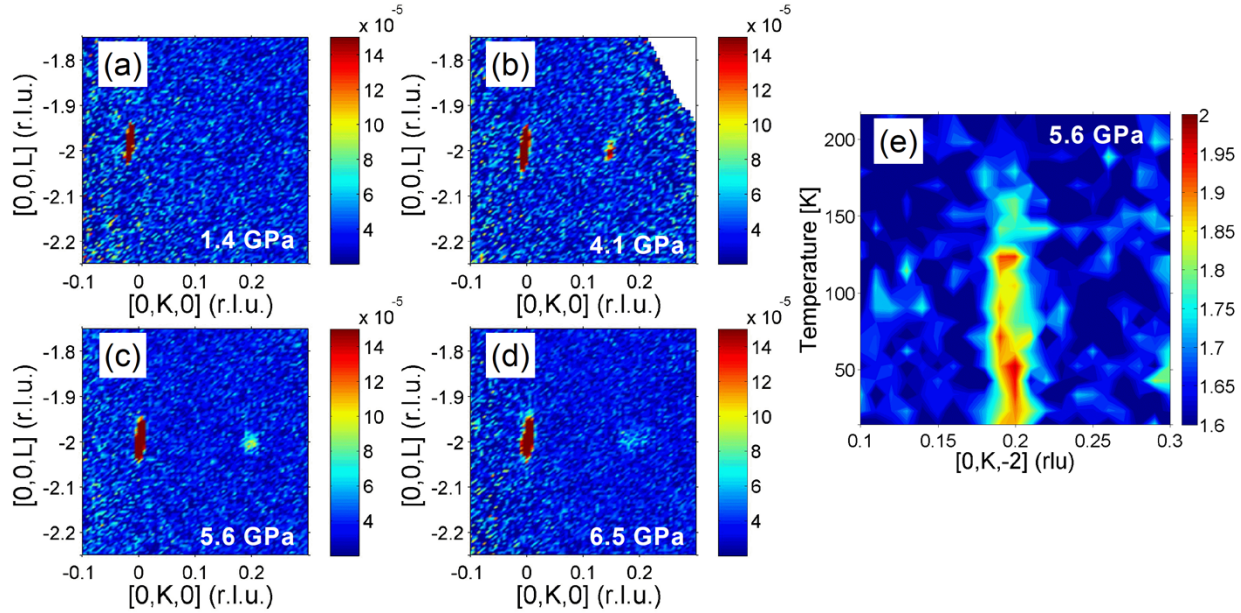
(a)
1.4 GPa
(b)
4.1 GPa
(c)
5.6 GPa
(d)
6.5 GPa
(e)
5.6 GPa
[0,0,L] (r.l.u.)
[0,K,0] (r.l.u.)
x 10^-5
Temperature [K]
[0,K,-2] (rlu)

Figure 4

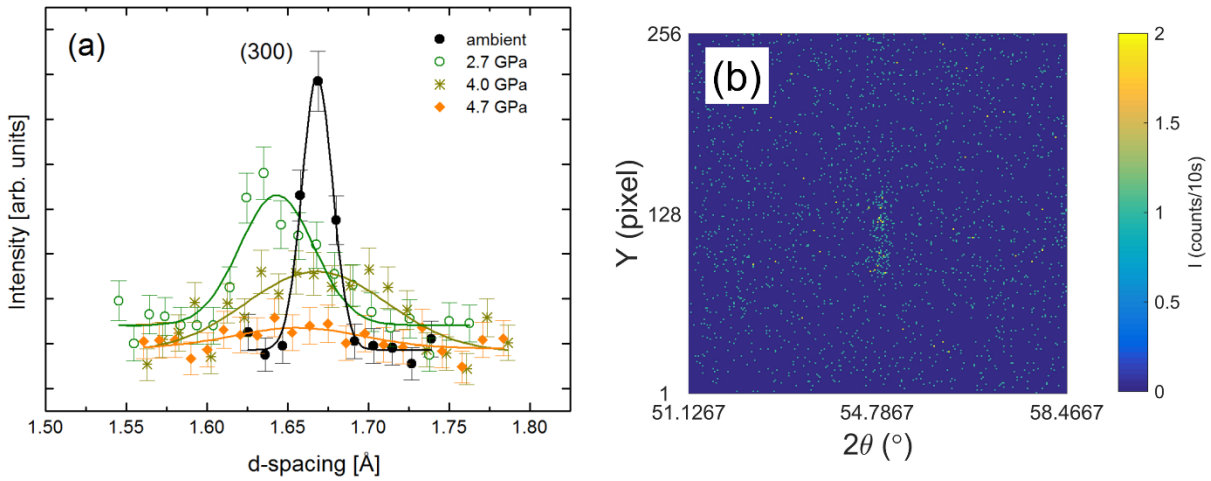
(a)
(300)
ambient
2.7 GPa
4.0 GPa
4.7 GPa
Intensity [arb. units]
1.50
1.55
1.60
1.65
1.70
1.75
1.80
d-spacing [Å]
(b)
256
128
1
Y (pixel)
51.1267
54.7867
58.4667
2θ (°)
2
1.5
1
0.5
0
I (counts/10s)

Figure 5

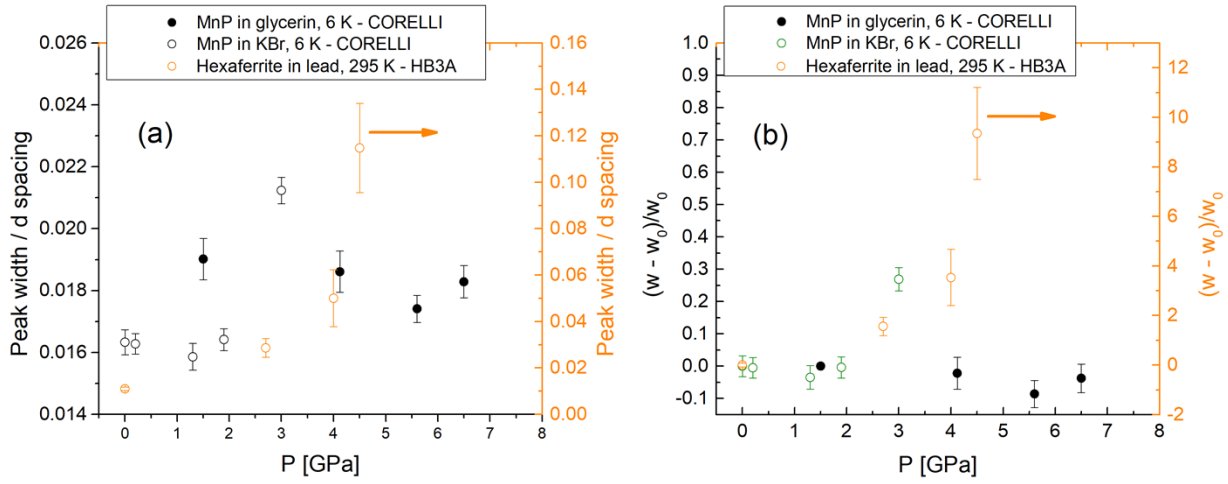
MnP in glycerin, 6 K - CORELLI
MnP in KBr, 6 K - CORELLI
Hexaferrite in lead, 295 K - HB3A
(a)
Peak width / d spacing
P [GPa]
(b)
(w - w0)/w0
P [GPa]

Figure 6

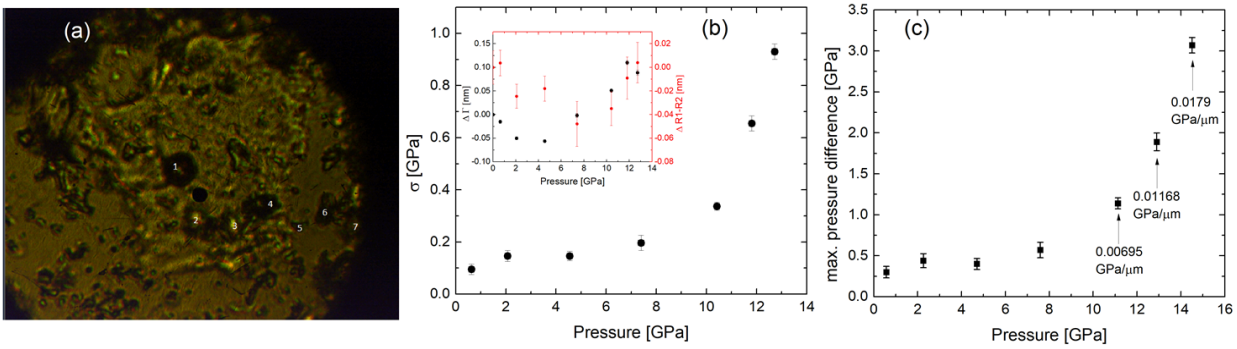
(a)
1
2
3
4
5
6
7
(b)
σ [GPa]
Pressure [GPa]
ΔT [nm]
ΔR1-R2 [nm]
(c)
max. pressure difference [GPa]
Pressure [GPa]
0.0179 GPa/μm
0.01168 GPa/μm
0.00695 GPa/μm

Figure 7

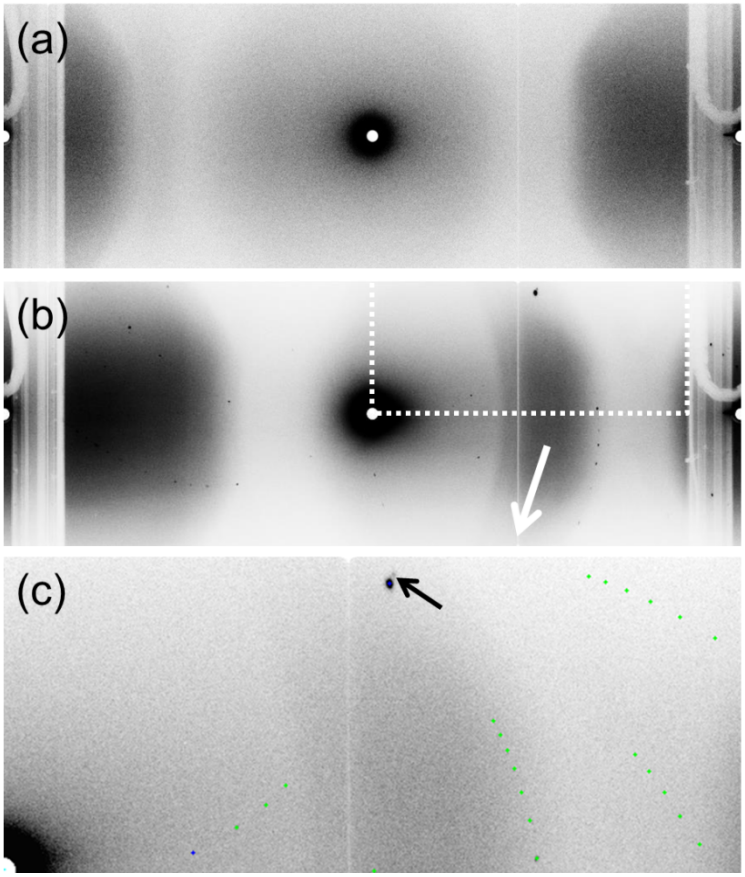

Figure 8

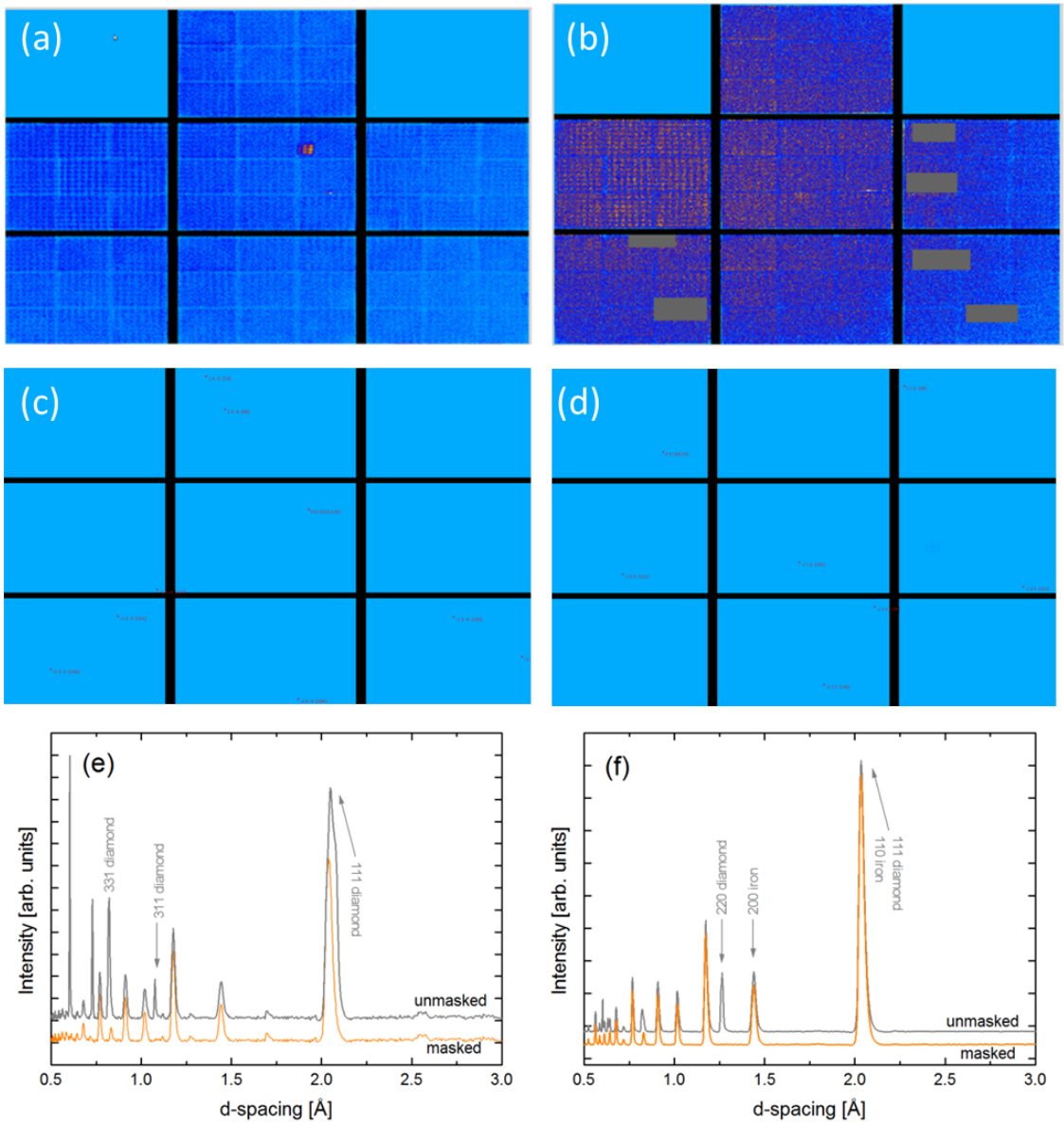
(a)
(b)
(c)
(d)
(e)
331 diamond
311 diamond
111 diamond
unmasked
masked
Intensity [arb. units]
d-spacing [Å]
0.5
1.0
1.5
2.0
2.5
3.0
(f)
220 diamond
200 iron
111 diamond
110 iron
unmasked
masked
Intensity [arb. units]
d-spacing [Å]